Introductory Tutorial on Nonlinear Modal Analysis Through an Academic Vibro-Impact Oscillator

Mathias Legrand

Introductory Tutorial on Nonlinear Modal Analysis Through an Academic Vibro-Impact Oscillator

Mathias Legrand
Structural Dynamics and Vibration Laboratory
Department of Mechanical Engineering
McGill University

Abstract This chapter is devoted to the nonlinear modal analysis of a nonsmooth academic vibro-impact oscillator. The aim is to introduce the classical ingredients of nonlinear modal analysis in a quasi-exact fashion. Periodic solutions, backbone curves in Frequency-Energy Plots, invariant manifolds, (grazing) bifurcation mechanisms, internal resonances, model-order reduction considerations and superabundance of nonlinear modes naturally emerge when solving the governing equations. Spectral stability analysis of (some) periodic orbits and time-domain solutions in their vicinity are also provided.

1 Introduction

Predicting the vibratory responses and dynamics of structures containing nonlinearities is an increasingly important research topic with potentially strong impact in the industrial sphere mainly because modal information is a crucial property of mechanical systems. This is the consequence of the recent development of new materials, the implementation of new efficient and lightweight designs along with the increasing computational capabilities of modern workstations. In effect, systems involving less damping and more structural flexibility are more susceptible to nonlinear mechanisms such as large deflections, unilateral contact and friction with neighbouring components and alike. The presence of such nonlinear and/or nonsmooth terms can give rise to a variety of behaviors such as frequency-energy dependence, internal resonances, and bifurcations to name a few.

Nonlinear modes of vibration are used in the study of nonlinear dynamical systems to describe the periodic motion of the system under the influence of nonlinear forces. In a linear system, a mode of vibration corresponds to a particular pattern of motion, characterized by a specific frequency and shape. In contrast, nonlinear systems can exhibit more complex vibratory behaviors, and the concept of mode needs to be extended to account for this complexity. In the present chapter, nonlinear modes are defined as one-parameter continuous families of periodic solutions of the system.

Studying nonlinear modes can provide insights into the behavior of nonlinear systems, including the existence of multiple possibly stable solutions, the influence of nonlinearities on the dynamical response, and the occurrence of mode coupling and energy transfer between modes. The literature on nonlinear modal analysis is always growing and this chapter is not designed to provide a thorough review in this area. Interested readers are referred to the other chapters of the present book, for instance (Touzé and Vizzaccaro, 2024; Thomas, 2024) or (Touzé et al., 2021; Renson et al., 2016) among others.

Instead, the present chapter briefly discusses recent developments on the modal analysis of structural systems subject to localized nonlinearities in the form of unilateral contact constraints and attendant impact laws. The main motivation is to provide closed-form expressions to the reader who is not familiar with the topic of nonlinear modal analysis. The contribution revisits existing works in this area (Legrand et al., 2017; Thorin et al., 2017) and exploits the welcome closed-form solutions to the dynamics in view of illustrating common features of nonlinear modes of vibration such as solution multiplicity (number of nonlinear modes is higher than the number of degrees-of-freedom, also called *modal superabundance*), bifurcation mechanisms, invariant manifolds and their parameterization, energy-frequency dependency, internal resonances and stability analysis. It also offers numerical insights into the intricate dynamics of systems with contact nonlinearities using a dedicated time-marching procedure. The chapter can be read as an introductory tutorial on nonlinear modal analysis without any prior knowledge and familiarity with the topic. Many features of nonlinear modes of vibration arise naturally and the proposed results can be reproduced without the use of advanced methodologies (serial expansions, multiple scale techniques, numerical time marching solutions, Ritz-Galerkin projections and alike).

Vibro-impact oscillators are mechanical systems that exhibit both oscillatory and impulsive responses. They commonly involve a system of connected oscillating masses, one of which being typically constrained to collide with a rigid *wall*. The impact results in a sudden change in momentum and energy transfer, leading to complex dynamic behaviors such as period doubling, chaos, and hysteresis loops in response to varying excitation frequencies or amplitudes. Considering such a system as an introductory example might seem counter-intuitive since unilateral contact constraints are commonly recognized to form a challenging class of nonlinearity, on both theoretical and numerical aspects. However, for the considered oscillator, the derivations dramatically simplify up to a point where quasi-exact solutions are available. This comes with a cost. The considered system is rather an academic toy without much physical relevance.

In order to efficiently distinguish between linear and nonlinear vibratory systems, an abuse of language is adopted in the form of *nonlinear natural frequency* versus *linear natural frequency*. It is surely understood that a natural frequency is neither nonlinear or linear, both terms referring to the underlying investigated system instead.

2 Simple one-degree-of-freedom impact oscillator

2.1 Governing equations

The very simple oscillator illustrated in Figure 1 is considered as an introductory example. It does not strictly comply with the aim of the present chapter in the sense that there is no notion of *mode of vibration* in the system. However, it embeds interesting nonlinear features that are classically reported in the field of nonlinear modal analysis. The two unknowns of the problem are

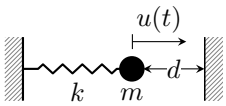

Figure 1. A generic 1-degree-of-freedom vibratory system with spring stiffness k and mass m, subject to a unilateral contact constraint.

the displacement $u(t)$ of the mass m and the reaction force $\lambda(t)$ induced by the presence of a rigid wall initially located at a distance d. The equations of motion read (Legrand et al., 2017)

$$m\ddot{u} + ku + \lambda = 0 \tag{1a}$$

$$d - u \geq 0, \quad \lambda \geq 0, \quad (d-u)\lambda = 0 \tag{1b}$$

$$u(t) = d \implies \dot{u}^+(t) = -\dot{u}^-(t). \tag{1c}$$

The classical initial conditions which commonly arise in such formulations are here omitted on purpose as they are not central to *modal analysis*. When contact closes, that is when $u(t) = d$, the presence of the rigid wall generates discontinuities in the velocity $\dot{u}(t)$, and thus impulses in the acceleration and the contact force. It is then required to define the pre- and post-impact velocities respectively denoted $\dot{u}^-$ and $\dot{u}^+$ in Equation (1c) and in the remainder of the present chapter.

The analysis is performed in terms of the value of (signed) initial gap d. The possible solutions are illustrated in Figure 2. It can be shown without difficulty that the solutions in the presence of

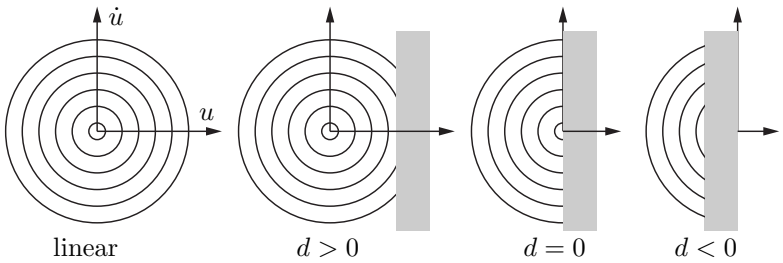

Figure 2. Phase diagrams for a simple one-degree-of-freedom vibro-impact oscillator with various initial gaps d.

the rigid are simply truncated versions of the solutions of the fully linear system, for all values of d. Trivially, the (linear) natural frequency of the (linear) oscillator (when the unilateral contact conditions are dismissed) is $\omega = \sqrt{k/m}$. Away from contact when $u(t) \leq d$ and $\lambda = 0$, it is

clear that $u(t) = A\cos\omega t + B\sin\omega t$ and $\dot{u}(t) = \omega(B\cos\omega t - A\sin\omega t)$. The rest of the analysis is developed below. It is essentially much easier than the analysis of the system for which the unilateral contact law is regularized, see for instance (Karkar et al., 2014) where appropriate approximations are detailed.

2.2 Comments on the impact law

For the unfamiliar reader, Equations (10a) and (10b) might seem to be sufficient to dictate the dynamics of the considered system, since two "equations" correspond to two unknowns (u and λ). However, it is well known that the multiple admissible solutions exist immediately after the time of contact closure, when $u(t) = d$. For instance, the second mass could immediately bounce back from the rigid foundation or remain on the rigid foundation for a certain amount of time, see Figure 3. In other words, contact closure can be seen as a mechanism which resets the *initial*

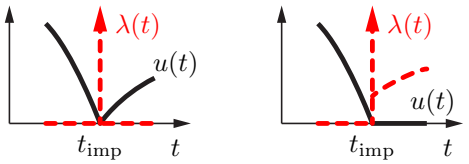

Figure 3. Two possible displacements of the contacting mass with respect to time, and corresponding contact forces, in the close vicinity of contact closure occurring at $t = t_{\text{imp}}$. The contact force has a Dirac impulse to enforce the mandatory discontinuity in the velocity (not shown). It also has a continuous component which is identically zero on the left but non-zero on the right after the contact closure when the mass rests on the rigid wall. Without a specified impact law, commonly in the form $\dot{u}^+ = -e\dot{u}^-$ where e is the coefficient of restitution, multiple admissible solutions satisfying the Signorini unilateral contact condition exist. In the present chapter, $e = 1$ by assumption.

velocity of the contacting mass, or post-impact velocity $\dot{u}^+(t)$ in Equation (10c), and infinitely many distinct post-contact velocities would generate solutions satisfying Equations (10a) and (10b). This non-uniqueness feature stems from the discrete nature of the considered oscillator, and more importantly from the rigid nature of the second mass. The rigid-body assumption for m ignores the constitutive law that would arise in the context of continuum mechanics where the body would then be able to distort. The cost to pay is on the non-uniqueness of the solutions. Another way to state the same is that in the context of continuum mechanics (the considered system would then be a simple one-dimensional bar in traction-compression, for instance), no inertia is involved in the boundary Signorini condition (10b). However, the semi-discretization procedure annihilates this property and the formulation in Equations (10a) and (10b) is not well-posed without an additional condition which enforced uniqueness. The latter commonly takes the form of an impact law, also known as a Newton impact law, Equation (10c) being one possible incarnation which preserves the kinetic energy of the system at all times. The undesired non-uniqueness issue arises in all semi-discretization schemes artificially "creating" mass on the contact boundary. The classical finite element procedure bears this deficiency, hence the envelopment of various dedicated methodologies (Khenous et al., 2008). However, the boundary element Method does not (Gimperlein et al., 2018). With all the above ingredients in mind, the nonlinear nature of the considered oscillator solely stems from the unilateral condition and more importantly here the time of contact closure which will be seen as the main unknown of the problem.

As indicated in Equation (10a), the contact force λ bears the same functional smoothness as the acceleration term $\ddot{u}$. Since the unilateral condition along with the impact law in Equations (10b) and (10c) directly act on the velocity $\dot{u}$ with a sudden change of sign, by a time-differentiation argument, it is clear that $\ddot{u}$ embeds the participation of a Dirac *generalized* function (or *distribution*) at the time of contact closure. Accordingly, it is expected to find a solution where u is at most a continuous function of time not everywhere differentiable in the classical sense, $\dot{u}$ is a piecewise continuous function of time with discontinuities at the times of contact closure and $\ddot{u}$ and λ are piecewise continuous functions of time with Dirac contributions.

2.3 Analysis in terms of the initial gap

In this subsection, a quantity of importance is the period T of an oscillation of (angular and nonlinear) frequency Ω with $\Omega T = 2\pi$.

Strictly positive initial gap A strictly positive initial gap $d > 0$ is assumed. From the general solution, we decide to choose the initial time $t = 0$ such that $u(0) = d = A$ and from the velocity jump assumed to occur at $t = T$, $\dot{u}^-(T) = -\dot{u}^+(0)$ which implies $-\omega d \sin \omega T + \omega B \cos \omega T = -\omega B$. This results into

$$B = \frac{d \sin \omega T}{\cos \omega T + 1} \tag{2}$$

and thus, for $t \in]0\,;T[$

$$\begin{aligned} u(t) &= d\Big(\cos \omega t + \frac{\sin \omega T}{\cos \omega T + 1} \sin \omega t\Big), \\ \dot{u}(t) &= \omega d\Big(\frac{\sin \omega T}{\cos \omega T + 1} \cos \omega t - \sin \omega t\Big). \end{aligned} \tag{3}$$

Once the system is specified (k, m and d are known along with $\omega = \sqrt{k/m}$ which should not be confused with Ω), the solution is solely parameterized in terms of the period T, remembering that the unilateral condition of non-penetration (1b) should also be satisfied, here *a posteriori*. The total energy of the system averaged on one period reads

$$E_{\text{av}}(T) = \frac{1}{T} \int_0^T \Big(\frac{1}{2} m \dot{u}(t)^2 + \frac{1}{2} k u(t)^2\Big)\, \mathrm{d}t = \frac{d^2 k}{1 + \cos \omega T} \tag{4}$$

and dictates the geometry of the backbone curve of the system of interest. Since the total energy is preserved in this conservative system, we can check that $E_{\text{av}}(T)$ is also the total energy at any time of the period and in particular at $t = 0$.

The backbone curve defines how the (natural) frequency Ω of the (nonlinear) oscillator is a function of the total energy $E_{\text{av}}(T(\Omega))$ of the response when neither damping nor forcing are present. Such backbone curves are conventionally shown in Frequency-Energy Plots, see Figure 4 where it is here chosen to indicate Ω on the horizontal axis and E_{av} on the vertical axis. From Equation (4), it

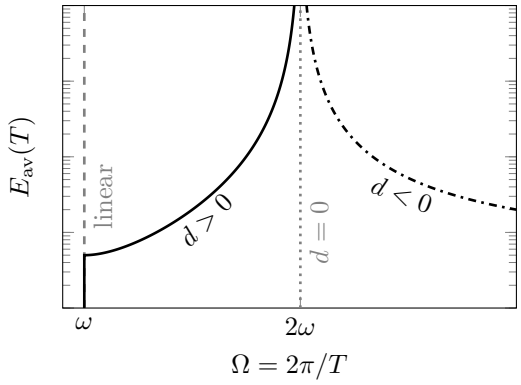

Figure 4. Backbone curve of the one-degree-of-freedom oscillator with $k = m = 1$ for various d values ($d = -1$, 0 and 1). For $d > 0$, the vertical portion of the branch shows linear solution before contact is initiated. The curved part indicates the Frequency-Energy dependence of the solutions satisfying the unilateral contact condition. Other parameterizations of the curve are possible, for instance using the initial velocity instead of the total energy.

is immediately clear that the backbone curve exhibits infinitely many branches separated by vertical asymptotes. However, only one of these branches with $\omega T \in [\pi, 2\pi]$ corresponds to admissible solutions located on the appropriate side (here, left) of the rigid wall. As a consequence, a stiffening behavior is experienced by the oscillator since the (natural) non-linear frequency increases with the averaged energy.

In a strictly equivalent fashion, it is also possible to rewrite the above by parameterizing the solution in terms of the initial velocity $\dot{u}^+(0)$ and enforcing the condition $u(0) = d$ at the very end. Using the requirement on the periodicity of the sough solution yields

$$\begin{pmatrix} u(T) \\ \dot{u}^-(T) \end{pmatrix} = \begin{bmatrix} \cos \omega T & \sin \omega T/\omega \\ -\omega \sin \omega T & \cos \omega T \end{bmatrix} \begin{pmatrix} u(0) \\ \dot{u}^+(0) \end{pmatrix} = \begin{pmatrix} u(0) \\ -\dot{u}^+(0) \end{pmatrix} \tag{5}$$

which translates into solving the *generalized* eigenvalue problem

$$\begin{bmatrix} \cos \omega T - 1 & \sin \omega T/\omega \\ -\omega \sin \omega T & \cos \omega T + 1 \end{bmatrix} \begin{pmatrix} u(0) \\ \dot{u}^+(0) \end{pmatrix} = \begin{pmatrix} 0 \\ 0 \end{pmatrix} \tag{6}$$

where the above matrix is always singular for all values of T and its kernel is thus non-empty and spanned by the vector

$$\begin{pmatrix} \dfrac{\sin\omega T}{\omega(1-\cos\omega T)} \\ 1 \end{pmatrix}. \tag{7}$$

Its magnitude is thus dictated by the condition $u(0) = d$. These derivations are similar to their counterparts for the two-degree-of-freedom system described in later sections.

Vanishing initial gap The case of an initially vanishing gap $d = 0$ is interesting because it shows how nonlinear systems may not be linearized in the classical way. We then speak of *essentially* nonlinear systems. Such systems also exist, at least mathematically, with smooth polynomial nonlinearities. We can think of a purely cubic spring for instance where the equation of motion would then read $\ddot{u} + \epsilon u^3 = 0$.

Using the above derivations with $d = 0$ leads to $A = 0$ and thus $u(t) = B\sin\omega t$. The jump condition on the velocity $\dot{u}^-(T) = -\dot{u}^+(0)$ implies $\omega B(\cos\omega T + 1) = 0$ with the condition $B \neq 0$ since the identically vanishing solution is not of interest. We should then solve the equation $\cos\omega T + 1 = 0$ which yields $\omega T = (2k+1)\pi$, $k = 0, 1, 2, \ldots$ and the general solution is thus

$$u(t) = B_k \sin(\omega t), \quad t \in]0\,; T_k[, \quad T_k = (2k+1)\pi/\omega, \quad k = 0, 1, 2\ldots \tag{8}$$

However, it is straightforward to check that only $k = 0$ yields an admissible solution as soon as $B_0 < 0$. The initially grazing one-degree-of-freedom impact oscillator features a unique nonlinear natural frequency $\Omega = 2\omega$ which is independent of the energy of the motion. In the Frequency-Energy Plot, the backbone curve is just a vertical line located at $\Omega = 2\omega$, see Figure 4 with corresponding orbits shown in Figure 2.

Negative initial gap A "negative" gap $d < 0$ means that the system is initially in a pre-stressed configuration possibly far from the configuration at rest. This case is also instructive. The equations are identical to the case $d > 0$ and Equation (4) is recovered. However, unilateral contact condition generates another unique admissible backbone curve branch, as shown in Figure 4. The backbone curve is unbounded when $\Omega \to \infty$.

This example shows in a very simple and natural manner how frequency and energy of an autonomous nonlinear oscillation are interrelated. It also illustrates the variety of possible periodic solutions experienced by a simple one-degree-of-freedom nonlinear impact oscillator.

3 Academic two-degree-of-freedom model

The dynamics of a two-degree-of-freedom vibro-impact system is much more intricate than that of the one-degree-of-freedom exposed above. Even more, there is no fundamental difference with a N-degree-of-freedom vibro-impact system. This is essentially a new world with many new dynamical features and open questions.

3.1 Governing equations

The periodic responses of a generic and academic, initially unstressed, autonomous and conservative two-degree-of-freedom vibro-impact oscillator illustrated in Figure 5 is investigated. The

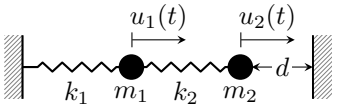

Figure 5. Generic two-degree-of-freedom vibratory system subject to a unilateral contact constraint.

two masses m_1 and m_2 and corresponding stiffnesses k_1 and k_2 are associated to the two physical displacements $u_1(t)$ and $u_2(t)$. The displacement $u_2(t)$ is subject to an impenetrability condition due to the presence of a rigid foundation located at a distance d from its equilibrium, here assumed to be strictly positive even though other configurations could also be considered, as suggested in the previous section.

The mass and stiffness matrices, stemming from a finite-element-based semi-discretization in space, are assumed to be

$$\mathbf{K} = \begin{bmatrix} 4 & -2 \\ -2 & 2 \end{bmatrix} \quad \text{and} \quad \mathbf{M} = \begin{bmatrix} 1/2 & 0 \\ 0 & 1/2 \end{bmatrix} \tag{9}$$

and the problem of interest reads: Find the displacement $\mathbf{u}(t) \equiv [u_1(t), u_2(t)]^\top$ and the contact force $\lambda(t)$ satisfying

$$\begin{bmatrix} 1/2 & 0 \\ 0 & 1/2 \end{bmatrix} \begin{pmatrix} \ddot{u}_1 \\ \ddot{u}_2 \end{pmatrix} + \begin{bmatrix} 4 & -2 \\ -2 & 2 \end{bmatrix} \begin{pmatrix} u_1 \\ u_2 \end{pmatrix} + \begin{bmatrix} 0 \\ 1 \end{bmatrix} \lambda = \begin{pmatrix} 0 \\ 0 \end{pmatrix} \tag{10a}$$

$$d - u_2 \geq 0, \quad \lambda \geq 0, \quad (d - u_2)\lambda = 0 \tag{10b}$$

$$u_2(t) = d \quad \Rightarrow \quad \dot{u}_2^+(t) = -\dot{u}_2^-(t). \tag{10c}$$

3.2 Periodic solutions with a single impact per period

Simplified formulation Given the above governing equations, where dissipative terms are omitted by choice, it seems quite natural to search for periodic autonomous solutions. However, the contact conditions might be challenging to satisfy. It is thus decided to simplify the formulation by targeting T-periodic solutions featuring only one impact per period. Such solutions might not exist, but as shown below, they actually do exist and have simple expressions. The main advantage of this simplification of one impact per period is the possibility to remove the quantity λ from the set of unknowns. The cost is that only a very small subset of all possible periodic solutions shall be captured and admissibility of the solutions will have to be (numerically) checked *a posteriori*. Accordingly, Problem (10) shall be reformulated and simplified as follows: Find T and $\mathbf{u}(t)$ such that:

$$\mathbf{M}\ddot{\mathbf{u}} + \mathbf{K}\mathbf{u} = \mathbf{0}, \quad \forall t \in]0\,;T[\tag{11a}$$

$$\mathbf{u}(T) = \mathbf{u}(0) \tag{11b}$$

$$u_2(0) = d \tag{11c}$$

$$\dot{\mathbf{u}}^-(T) = \mathbf{S}\dot{\mathbf{u}}^+(0) \tag{11d}$$

where the jump matrix

$$\mathbf{S} = \begin{bmatrix} 1 & 0 \\ 0 & -1 \end{bmatrix} \tag{12}$$

enforces the impact law on the contacting mass and guarantees velocity continuity on the other mass. In Equation (11), the unilateral Signorini condition (10b) is discarded by choice but solutions to Equation (11) might violate Equation (10b), in which case they would be deemed *inadmissible* solutions. In short, System (11) says the following:

- Without loss of generality, contact closure is assumed to occur at $t = T$ so that Equations (11b) and (11c) hold.
- Away from a contact closure, the system is free and its dynamics is governed by Equation (11a).
- The displacement is a continuous and periodic function of time.
- The period T is an unknown of the problem.
- The velocity of mass 2 is discontinuous at $t = T$ where it satisfies $\dot{u}_2^+(T) = -\dot{u}_2^-(T)$.

Of interest are one-parameter continuous families of periodic solutions. If such families exist, they will be organized on two-dimensional invariant manifolds which usually characterize modes of vibration for nonlinear mechanical systems.

Quasi-exact solutions In order to exhibit an almost closed-form expression of the solution displacement, Equation (11a) is projected onto the linear modal space through the transformation $\mathbf{u} = \mathbf{P}\mathbf{q}$, and thus $\dot{\mathbf{u}} = \mathbf{P}\dot{\mathbf{q}}$, to become

$$\mathbf{I}\ddot{\mathbf{q}} + \mathbf{\Omega}^2\mathbf{q} = \mathbf{0} \tag{13}$$

where

$$\mathbf{q}(t) \equiv \begin{pmatrix} q_1(t) \\ q_2(t) \end{pmatrix}, \quad \mathbf{I} = \begin{bmatrix} 1 & 0 \\ 0 & 1 \end{bmatrix} \quad \text{and} \quad \mathbf{\Omega} = \begin{bmatrix} \omega_1 & 0 \\ 0 & \omega_2 \end{bmatrix} \tag{14}$$

with $\omega_1 = \sqrt{2}\sqrt{3 - \sqrt{5}} \approx 1.236$ and $\omega_2 = \sqrt{2}\sqrt{3 + \sqrt{5}} \approx 3.236$. The matrix of $\mathbf{M}$-normalized eigenvectors stored columnwise reads

$$\mathbf{P} = \frac{1}{\sqrt{5 - \sqrt{5}}} \begin{bmatrix} 1 - \sqrt{5} & -2 \\ -2 & \sqrt{5} - 1 \end{bmatrix} \tag{15}$$

and the change of basis expressed in the state-space is

$$\begin{pmatrix}\mathbf{u}\\ \dot{\mathbf{u}}\end{pmatrix} = \begin{bmatrix}\mathbf{P} & \mathbf{0}\\ \mathbf{0} & \mathbf{P}\end{bmatrix}\begin{pmatrix}\mathbf{q}\\ \dot{\mathbf{q}}\end{pmatrix} \tag{16}$$

as classically known for the system of interest which features no velocity terms in the governing equations (for instance, no viscous damping or gyroscopic terms). The matrix of eigenvectors is such that $\mathbf{P}^{-1} = \mathbf{P}^{\top}\mathbf{M} = \mathbf{P}\mathbf{M} = \frac{1}{2}\mathbf{P}$. From Equation (13), it is straightforward to map the state of system at $t = 0^+$ to its state at $t = T^-$ through

$$\mathbf{q}^-(T) = \mathbf{cos}(T\boldsymbol{\Omega})\mathbf{q}^+(0) + \boldsymbol{\Omega}^{-1}\,\mathbf{sin}(T\boldsymbol{\Omega})\dot{\mathbf{q}}^+(0) \tag{17a}$$

$$\dot{\mathbf{q}}^-(T) = -\boldsymbol{\Omega}\,\mathbf{sin}(T\boldsymbol{\Omega})\mathbf{q}^+(0) + \mathbf{cos}(T\boldsymbol{\Omega})\dot{\mathbf{q}}^+(0) \tag{17b}$$

where

$$\mathbf{cos}(t\boldsymbol{\Omega}) \equiv \begin{bmatrix}\cos\omega_1 t & 0\\ 0 & \cos\omega_2 t\end{bmatrix} \text{ and } \mathbf{sin}(t\boldsymbol{\Omega}) \equiv \begin{bmatrix}\sin\omega_1 t & 0\\ 0 & \sin\omega_2 t\end{bmatrix} \tag{18}$$

are used as notations. In modal coordinates, the expression of the jump matrix is

$$\boldsymbol{\mathcal{S}} = \mathbf{P}^{-1}\mathbf{S}\mathbf{P} = \tfrac{1}{2}\mathbf{P}\mathbf{S}\mathbf{P} = \frac{1}{\sqrt{5}}\begin{bmatrix}-1 & 2\\ 2 & 1\end{bmatrix} \tag{19}$$

and the continuity of both displacements and the velocity of the non-contacting mass along with the velocity jump of the impacting mass occurring at $t = T$ collectively read

$$\mathbf{q}^+(T) = \mathbf{q}^-(T) \tag{20a}$$

$$\dot{\mathbf{q}}^+(T) = \boldsymbol{\mathcal{S}}\dot{\mathbf{q}}^-(T). \tag{20b}$$

When T is known and by inserting Equation (17) into Equation (20), a 4×4 matrix $\mathbf{R}(T)$ mapping the system from $t = 0^+$ to $t = T^+$ can be built in modal coordinates. It includes the free flight as well as one impact at $t = T$:

$$\begin{pmatrix}\mathbf{q}(T)\\ \dot{\mathbf{q}}^+(T)\end{pmatrix} = \begin{bmatrix}\mathbf{cos}(T\boldsymbol{\Omega}) & \boldsymbol{\Omega}^{-1}\,\mathbf{sin}(T\boldsymbol{\Omega})\\ -\boldsymbol{\mathcal{S}}\boldsymbol{\Omega}\,\mathbf{sin}(T\boldsymbol{\Omega}) & \boldsymbol{\mathcal{S}}\,\mathbf{cos}(T\boldsymbol{\Omega})\end{bmatrix}\begin{pmatrix}\mathbf{q}(0)\\ \dot{\mathbf{q}}^+(0)\end{pmatrix}. \tag{21}$$

which becomes, in physical coordinates

$$\begin{pmatrix}\mathbf{u}(T)\\ \dot{\mathbf{u}}^+(T)\end{pmatrix} = \begin{bmatrix}\mathbf{P}\,\mathbf{cos}(T\boldsymbol{\Omega})\mathbf{P}^{-1} & \mathbf{P}\boldsymbol{\Omega}^{-1}\,\mathbf{sin}(T\boldsymbol{\Omega})\mathbf{P}^{-1}\\ -\mathbf{S}\mathbf{P}\boldsymbol{\Omega}\,\mathbf{sin}(T\boldsymbol{\Omega})\mathbf{P}^{-1} & \mathbf{S}\mathbf{P}\,\mathbf{cos}(T\boldsymbol{\Omega})\mathbf{P}^{-1}\end{bmatrix}\begin{pmatrix}\mathbf{u}(0)\\ \dot{\mathbf{u}}^+(0)\end{pmatrix}. \tag{22}$$

A periodic one-impact-per-period is shown in Figure 6 as an example.

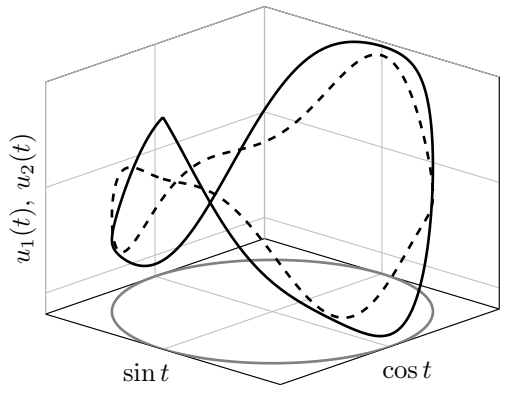

Figure 6. One-impact-per-period periodic orbit at $\Omega \approx \omega_2/4$: $u_2(t)$ [solid line] and $u_1(t)$ [dashed line].

3.3 Manifold parameterization

It is interesting to look at the dynamics through the concept of nonlinear normal modes. Since the considered dynamics is undamped, a nonlinear mode of vibration is equivalently defined as an invariant manifold or a family of periodic orbits (Thomas, 2024; Touzé and Vizzaccaro, 2024). The

invariant manifold can be computed through dedicated parametrisation and change of variables that work for smooth nonlinearities. However, the second definition (family of periodic orbits) can be used to define and then compute invariant manifolds using various techniques, ranging from analytical to numerical strategies. In the present work, such parameterizations are challenging, if not impossible. However, a quasi-exact solution in terms of time t and period T can be achieved. The question is to characterize the kernel of the operator

$$\begin{bmatrix} \mathbf{P}\cos(T\mathbf{\Omega})\mathbf{P}^{-1} - \mathbf{I} & \mathbf{P}\mathbf{\Omega}^{-1}\sin(T\mathbf{\Omega})\mathbf{P}^{-1} \\ -\mathbf{S}\mathbf{P}\mathbf{\Omega}\sin(T\mathbf{\Omega})\mathbf{P}^{-1} & \mathbf{S}\mathbf{P}\cos(T\mathbf{\Omega})\mathbf{P}^{-1} - \mathbf{I} \end{bmatrix}. \tag{23}$$

It can be shown that the following quantities are well defined (Legrand et al., 2017):

$$\mathbf{\Phi}(T) = \mathbf{\Omega}^{-1}(\mathbf{I} - \cos(T\mathbf{\Omega}))^{-1}\sin(T\mathbf{\Omega}) \tag{24a}$$

$$\mathbf{w}(T) = (\mathbf{P}\mathbf{\Phi}(T)\mathbf{P}^{-1})\mathbf{e}_2 \tag{24b}$$

$$w_2(T) = \mathbf{e}_2^\top \mathbf{w}(T) \tag{24c}$$

where $\mathbf{e}_2 \equiv [0\ 1]^\top$, which then leads to

$$\begin{pmatrix} \mathbf{u}(0) \\ \dot{\mathbf{u}}^+(0) \end{pmatrix} = \begin{bmatrix} \mathbf{P} & \mathbf{0} \\ \mathbf{0} & \mathbf{P} \end{bmatrix} \begin{pmatrix} \mathbf{q}(0) \\ \dot{\mathbf{q}}^+(0) \end{pmatrix} = c \begin{pmatrix} \mathbf{w}(T) \\ \mathbf{e}_2 \end{pmatrix}. \tag{25}$$

where c is uniquely specified by the condition $u_2(0) = d$. The solution in Equation (25) can be seen as the "shape" $\mathbf{w}(T)$ of the mode (as commonly found for linear modes that are standing waves) to which is added an initial velocity on the second degree-of-freedom.

For the system of interest, the different quantities are expanded as follows:

$$\mathbf{\Phi}(T) = \begin{bmatrix} \dfrac{\sin\omega_1 T}{\omega_1(1-\cos\omega_1 T)} & 0 \\ 0 & \dfrac{\sin\omega_2 T}{\omega_2(1-\cos\omega_2 T)} \end{bmatrix} \tag{26}$$

and

$$\mathbf{w}(T) = \begin{pmatrix} \dfrac{(\sqrt{5}-1)(\omega_2\sin\omega_1 T(\cos\omega_2 T - 1) - \omega_1(\cos\omega_1 T - 1)\sin\omega_2 T)}{(\sqrt{5}-5)\omega_1\omega_2(\cos\omega_1 T - 1)(\cos\omega_2 T - 1)} \\ \dfrac{2(\sqrt{5}-3)\omega_1\sin^2(T\omega_1/2)\sin\omega_2 T - 4\omega_2\sin\omega_1 T\sin^2(T\omega_2/2)}{(\sqrt{5}-5)\omega_1\omega_2(\cos\omega_1 T - 1)(\cos\omega_2 T - 1)} \end{pmatrix} \tag{27}$$

which is proportional to the initial displacements of the oscillator initiating a periodic orbit with one impact per period. Inserting the initial condition

$$\begin{pmatrix} u_1(0) \\ u_2(0) \\ \dot{u}_1(0) \\ \dot{u}_2^+(0) \end{pmatrix} = \frac{g}{w_2(T)} \begin{pmatrix} \dfrac{(\sqrt{5}-1)(\omega_2\sin\omega_1 T(\cos\omega_2 T - 1) - \omega_1(\cos\omega_1 T - 1)\sin\omega_2 T)}{(\sqrt{5}-5)\omega_1\omega_2(\cos\omega_1 T - 1)(\cos\omega_2 T - 1)} \\ \dfrac{2(\sqrt{5}-3)\omega_1\sin^2(T\omega_1/2)\sin\omega_2 T - 4\omega_2\sin\omega_1 T\sin^2(T\omega_2/2)}{(\sqrt{5}-5)\omega_1\omega_2(\cos\omega_1 T - 1)(\cos\omega_2 T - 1)} \\ 0 \\ 1 \end{pmatrix} \tag{28}$$

or equivalently

$$\begin{pmatrix} u_1(0) \\ u_2(0) \\ \dot{u}_1(0) \\ \dot{u}_2^+(0) \end{pmatrix} = d \begin{pmatrix} \dfrac{(\sqrt{5}-1)(\omega_2\sin\omega_1 T(\cos\omega_2 T - 1) - \omega_1(\cos\omega_1 T - 1)\sin\omega_2 T)}{2(\sqrt{5}-3)\omega_1\sin^2(T\omega_1/2)\sin\omega_2 T - 4\omega_2\sin\omega_1 T\sin^2(T\omega_2/2)} \\ 1 \\ 0 \\ \dfrac{(\sqrt{5}-5)\omega_1\omega_2(\cos\omega_1 T - 1)(\cos\omega_2 T - 1)}{2(\sqrt{5}-3)\omega_1\sin^2(T\omega_1/2)\sin\omega_2 T - 4\omega_2\sin\omega_1 T\sin^2(T\omega_2/2)} \end{pmatrix} \tag{29}$$

into Equation (22) provides one possible parameterization of the invariant manifold in (t, T) with $t \in]0\,;T[$ which can be expressed as

$$\begin{pmatrix} \mathbf{u}(t;T) \\ \dot{\mathbf{u}}^+(t;T) \end{pmatrix} = \frac{d}{w_2(T)} \begin{pmatrix} \mathbf{P}(\cos(t\mathbf{\Omega})\mathbf{\Phi}(T) + \mathbf{\Omega}^{-1}\sin(t\mathbf{\Omega}))\mathbf{P}^{-1} \\ \mathbf{S}\mathbf{P}(\cos(t\mathbf{\Omega}) - \mathbf{\Omega}\sin(t\mathbf{\Omega})\mathbf{\Phi}(T))\mathbf{P}^{-1} \end{pmatrix} \mathbf{e}_2. \tag{30}$$

In the expression "one-parameter continuous families of periodic solutions", the period T in Equation (30) plays the role of the parameter in question while t plays the role of the parameter

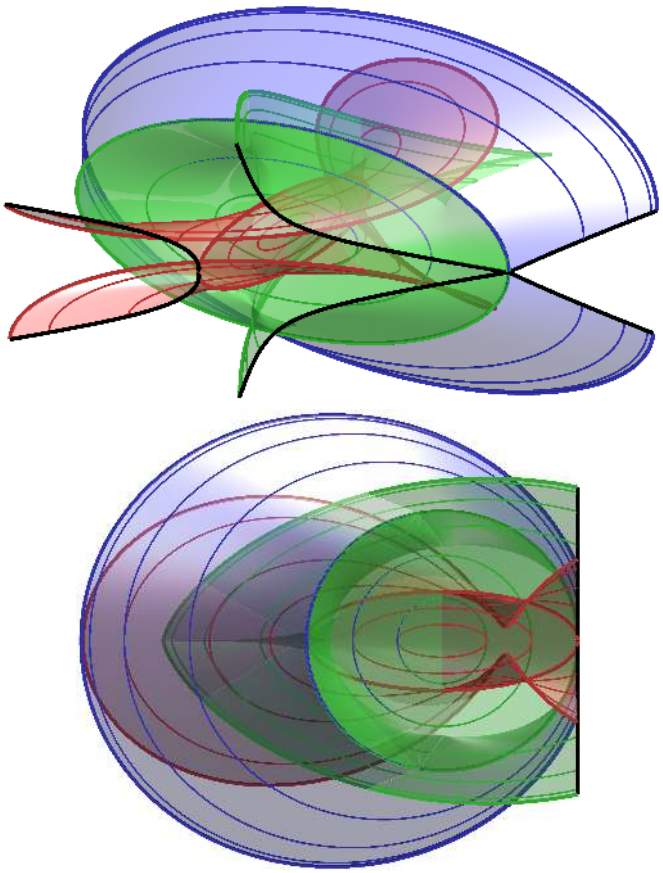

Figure 7. Invariant manifolds projected on $(u_1, u_2, \dot{u}_2)$ and parameterized in (t, T) for a positive initial gap d (3D and front views). Only truncated versions are shown within the respective admissible region. The blue and green manifolds share the same linear portion which is the second linear mode shown as the green flat ellipse. The red manifold corresponds to the first linear mode. A few orbits populating the manifolds are also shown. The green and blue manifolds emerge from the same linear mode through a grazing bifurcation mechanism. The red and green ellipses show the orientation of the linear modal subspaces of the unconstrained system. Their common center is the rest configuration of the system. Note that manifolds also exist in the vicinity of the sub-harmonics ω_1/m and ω_2/p, m and p being strictly positive integers.

for the periodic solutions. Note that, from Equation (29), $\dot{u}_1$ vanishes when the second mass hits the wall. An example of such manifolds is illustrated in Figure 7. As explained in (Thomas, 2024; Touzé and Vizzaccaro, 2024) (and attendant cited works), this type of parameterization is unusual. It here has the crucial advantage of being exact within the admissibility interval. However, it is in general more common to develop invariant manifold parameterizations that are independent of time using the concept of master coordinates suggested above. It is here theoretically possible, at least locally through the Implicit Function theorem, by inverting the relevant entries of Equation (30) in order to express the pair (t, T) in terms of the pair $(u_1, \dot{u}_1)$ subsequently inserted in the expressions of $(u_2, \dot{u}_2)$. However, this is a really challenging if not an impossible task in practice. Locally, in the vicinity of the grazing linear solutions, trigonometric functions cos and sin could be Taylor-expanded using the identities $\omega_1 T \approx 2\pi$ or $\omega_2 T \approx 2\pi$ for modes 1 and 2, respectively, but this exercise has not been attempted.

The manifolds shown in Figure 7 are the three-dimensional "shadows", or projections, of two-dimensional manifolds embedded in a four-dimensional state-space. In the plot, the fact that the second linear mode bifurcates into the blue and green invariant manifolds (and actually many, possibly countably infinitely many) is a sign of *superabundance* of nonlinear modes, which simply says that the number of nonlinear modes can exceed the number of degrees-of-freedom which is obviously impossible in a linear context.

Based on Equation (30) evaluated at $t = 0$, it is possible to get the expression of the corresponding total energy of the motion for every T and then the corresponding backbone curves in the Frequency-Energy plot, see Figure 8.

In order to estimate the participation of the modes in the computed nonlinear responses,

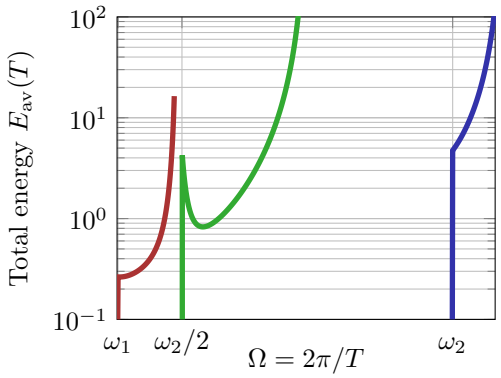

Figure 8. Frequency-Energy Plot showing the three backbone curves of three admissible one-impact-per-period solutions located in the vicinity of $\Omega = \omega_1$, $\Omega = \omega_2/2$ and $\Omega = \omega_2$. The green and blue backbone curves are not bounded in energy. However, the red backbone curve becomes non-admissible at a point where a three-impact-per-period solution emerges (not shown).

normalized modal contributions are approximated as

$$q_{1\text{n}} \equiv \frac{q_1^2(0) + \dot{q}_1^2(0)}{q_1^2(0) + \dot{q}_1^2(0) + q_2^2(0) + \dot{q}_2^2(0)} \text{ and } q_{2\text{n}} \equiv \frac{q_2^2(0) + \dot{q}_2^2(0)}{q_1^2(0) + \dot{q}_1^2(0) + q_2^2(0) + \dot{q}_2^2(0)}. \tag{31}$$

and indicated in Figure 9. They reach one only when the corresponding linear mode is participating

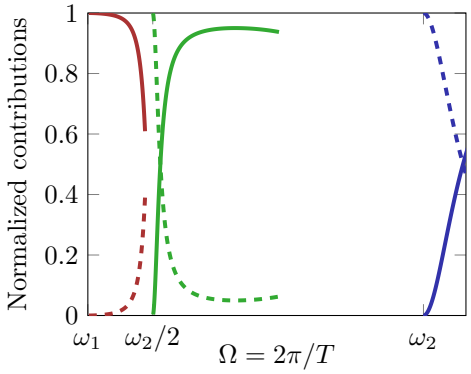

Figure 9. Normalized modal contributions in the periodic solutions within the admissibility domain: [solid] $q_{1\text{n}}$, [dashed] $q_{2\text{n}}$.

in the solution, and vice-versa. As expected, the grazing nonlinear solution at $\omega_j T \approx 2\pi$, $j = 1, 2$ is dominated by the corresponding mode, that is mode 1 in the vicinity of $\Omega = \omega_1$ and mode 2 in the vicinity of $\Omega = \omega_2/2$ or $\Omega = \omega_2$. In case one of these coefficients reaches unity for a given Ω away from the linear grazing solutions, the nonlinear solution is a sole linear mode seen on a truncated period of time, similar to the one-degree-of-freedom case detailed in Section 2, see Figure 2.

3.4 Reduced-order modeling

Nonlinear modes of vibration are known to offer a well-established framework for reducing the dynamics of nonlinear systems. In a linear context, in a particular operating range, the system is assumed to operate with a few modal participations being active or dominant. Mathematically, the system operates in flat (or linear) subspaces of small dimension in the state-space. This principle readily extends to nonlinear systems at the cost of (1) a "distortion" of the subspaces in the form of "curved" invariant manifolds and (2) having the Principle of Superposition no longer operational. For the considered two-degree-of-freedom vibro-impact system with a state-space of dimension 4, the dynamics realized on the manifolds is governed by two independent variables and thus model reduction is achieved. However, as already discussed, the (t, T)-parameterization which naturally emerges during the construction of the manifolds is not exactly adapted to the construction of an explicit reduced-order model in the form of a single pair of first-order Ordinary Differential Equations in the master coordinates, as it is commonly achieved for smooth nonlinear systems.

3.5 Stability analysis

Although periodic orbits (and thus modes of vibration) of linear conservative systems are known to be neutrally stable, the situation differs in nonlinear systems. Using the notation $\mathbf{U}_t := (\mathbf{u}(t), \dot{\mathbf{u}}^+(t))$, the stability analysis of a periodic orbit of initial conditions $\mathbf{U}_0$ of period T_0 lying on the previously constructed manifolds can be assessed by measuring how a slightly perturbed initial condition $\mathbf{U}_0 + \delta\mathbf{U}_0$ lying on the Poincaré section $u_2(t) = d$ is mapped back onto the Poincaré section through $\mathbf{U}_T = \mathbf{U}_0 + \delta\mathbf{U}_T$ after a time $T = T_0 + \delta T$ with the condition $\bar{\mathbf{e}}_4^\top \, \delta\mathbf{U}_T = 0$ and notation $\bar{\mathbf{e}}_4 \equiv [0 \ 1 \ 0 \ 0]^\top$. In equivalent terms, we want to quantify how a perturbation $\delta\mathbf{U}_0$ magnifies into $\delta\mathbf{U}_T$. If its amplitude is magnified, then the periodic orbit said to be *unstable*. This spectral stability analysis relies on the smoothness of the mapping (22) as a function of the initial conditions and the period (itself function of the initial conditions) but fails to be correct for grazing orbits. In a compact matrix format, this mapping evaluated at a one-impact-per-period solution reads

$$\mathbf{U}_0 = \mathbf{\Gamma}(T_0)\mathbf{U}_0. \tag{32}$$

An admissible perturbed orbit thus satisfies

$$\mathbf{U}_0 + \delta\mathbf{U}_T = \mathbf{\Gamma}(T_0 + \delta T)(\mathbf{U}_0 + \delta\mathbf{U}_0). \tag{33}$$

Neglecting higher-order terms and using Equation (32), Equation (33) simplifies to

$$\delta\mathbf{U}_T = \mathbf{\Gamma}(T_0)\delta\mathbf{U}_0 + \delta T\dot{\mathbf{\Gamma}}(T_0)\mathbf{U}_0 \tag{34}$$

where $\dot{\mathbf{\Gamma}}$ denotes the derivative of $\mathbf{\Gamma}$ with respect to its argument and has the expanded form

$$\dot{\mathbf{\Gamma}}(T) = \begin{bmatrix} -\mathbf{P}\mathbf{\Omega}\,\mathbf{sin}(T\mathbf{\Omega})\mathbf{P}^{-1} & \mathbf{P}\,\mathbf{cos}(T\mathbf{\Omega})\mathbf{P}^{-1} \\ -\mathbf{S}\mathbf{P}\mathbf{\Omega}^2\,\mathbf{cos}(T\mathbf{\Omega})\mathbf{P}^{-1} & -\mathbf{S}\mathbf{P}\mathbf{\Omega}\,\mathbf{sin}(T\mathbf{\Omega})\mathbf{P}^{-1} \end{bmatrix}. \tag{35}$$

Using the fact that $\mathbf{e}_2^\top \, \delta\mathbf{u}(T) = \mathbf{e}_2^\top \, \delta\mathbf{u}(T_0) = 0$, it is possible to write (Legrand et al., 2017)

$$\delta T = -\frac{\bar{\mathbf{e}}_4^\top \mathbf{\Gamma}(T_0)\delta\mathbf{U}_0}{\bar{\mathbf{e}}_4^\top \dot{\mathbf{\Gamma}}(T_0)\mathbf{U}_0} \tag{36}$$

and System (34) thus simplifies to

$$\delta\mathbf{U}_T = \Big(\mathbf{\Gamma}(T_0) - \frac{\dot{\mathbf{\Gamma}}(T_0)\mathbf{U}_0\bar{\mathbf{e}}_4^\top \mathbf{\Gamma}(T_0)}{\bar{\mathbf{e}}_4^\top \dot{\mathbf{\Gamma}}(T_0)\mathbf{U}_0}\Big)\delta\mathbf{U}_0. \tag{37}$$

For a given periodic response, a sufficient condition for instability is that at least one of the eigenvalues in modulus, of the matrix arising in Equation (37), lies outside the unit circle in the complex plane. Perturbations of an unstable periodic orbit deviate from it in the state-space but remain on the ellipsoid of constant energy specified by the initial conditions. In contrast, stable periodic orbits will see their perturbations stay in their vicinity at all times.

In order to quickly observe the dynamics in the vicinity of an orbit lying on a nonlinear mode invariant manifold, a basic Moreau-Jean type time-stepping scheme (Acary and Brogliato, 2008) adapted from (Kern, 2019) is implemented, see Algorithm 1. In all simulations, $d = 1$, the time-step is $h = 10^{-6}$ s, the total number of iterations is $N = 2 \cdot 10^{10}$ and the beginning to the end is indicated from red to black points. The initial conditions are those of the investigated periodic orbit up to machine precision without any additional perturbation. Instability, if any, is initiated by machine round-off errors.

A chaotic-like solution in the vicinity of the linear grazing orbit of mode 1 is shown in Figure 11. The dynamics in the vicinity of a neutrally stable orbit is shown in Figure 12 and the dynamics in the vicinity of an unstable orbit is shown in Figure 13. These time-domain results come as a complement of the spectral stability analysis indicated in Figure 10. The energy is well preserved by the time-marching algorithm since all points lie on the ellipsoid of constant energy. However, even though a convergence analysis was conducted with $h = 10^{-5}$ s and $h = 10^{-7}$ s to confirm the correctness of the provided plots, these results should be considered with care as a full investigation will various time-stepping strategies would be required to conclude.

3.6 Internal resonances

Internal resonances are typical of nonlinear vibratory systems and correspond to a transfer of energy between various modes. They have no counterparts in linear dynamics. The literature is vast on the topic and the reader is again referred to (Thomas, 2024) for more information. The truly

Require 2×2 Mass and stiffness matrices $\mathbf{M}$ and $\mathbf{K}$; $m \leftarrow \mathbf{M}_{22}$
Require Time-step size: h; Total number of time steps: N
Require Initial gap: $d \leftarrow 1$; Restitution coefficient: $e \leftarrow 1$
Require Initial displacement $\mathbf{u}_0$ and velocity $\mathbf{v}_0$

for k from 1 to N **do**
  $\mathbf{u}_k \leftarrow \mathbf{u}_{k-1} + h\mathbf{v}_{k-1}$ ▷ Displacement update through Forward Euler
  $\mathbf{f} \leftarrow -h\mathbf{K}\mathbf{u}_k$ ▷ Corresponding internal force
  $\mathbf{v}_k \leftarrow \mathbf{v}_{k-1} + \mathbf{M}^{-1}\mathbf{f}$ ▷ Velocity update through Backward Euler assuming no contact
  if $u_{2;k} \geq d$ **then** ▷ Penetration detected then solve LCP in velocity
    $\mathrm{d}v \leftarrow -(1+e)v_{2;k}$ ▷ Velocity jump
    if $m\,\mathrm{d}v < f_{2;k}$ **then** ▷ Contact force has the correct sign
      $v_{2;k} \leftarrow v_{2;k-1} + \mathrm{d}v$ ▷ Velocity Correction for the contacting mass
    end if
  end if
end for

Algorithm 1: Simplified Moreau-Jean type time-marching solution method for two-degree-of-freedom vibro-impact oscillator. Vector notation at time iteration k: $\mathbf{a}_k \equiv [a_{1;k}\, a_{2;k}]^\top$.

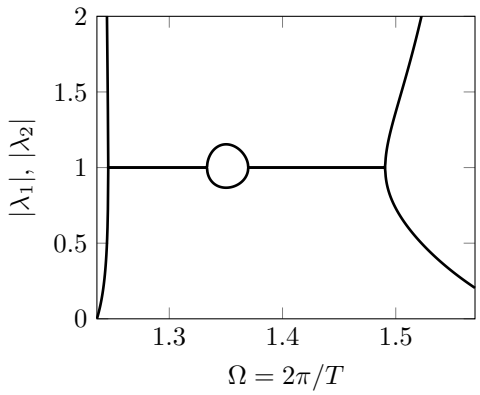

Figure 10. Spectral stability analysis along the backbone curve of mode 1. An eigenvalue modulus larger than unity indicates instability of the periodic orbit. Note that the two other eigenvalues 0 and 1 are discarded, see (Legrand et al., 2017).

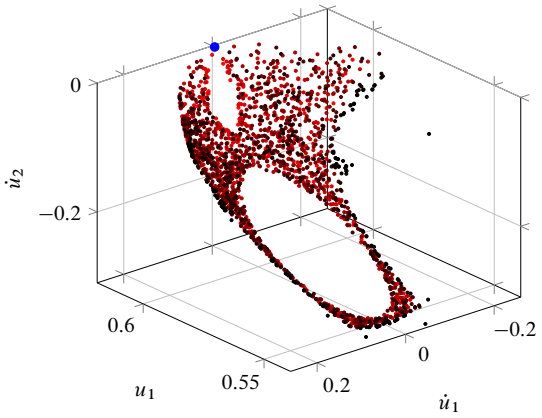

Figure 11. Post-impact Poincaré section at t^+_{imp} in the vicinity of the linear grazing orbit at $\Omega = 1.2361$. Initial condition indicated as a blue dot. In agreement with Figure 10, the grazing orbit seems to be unstable (although the question is still open theoretically for that specific solution) and surrounded by chaotic responses.

nonlinear mechanism arises when (linear and/or nonlinear) frequencies of vibration are multiples of each other, that is when $m\omega_1 = p\omega_2$, for some strictly positive integers m, p for the system of interest. Although it is not necessarily straightforward to design a chain-like two-degree-of-freedom oscillator with internal resonances, it is possible to think about two distinct one-degree-of-freedom oscillators interacting with each other through a unilateral condition, as illustrated in Figure 14. The stiffness and mass matrices are diagonal:

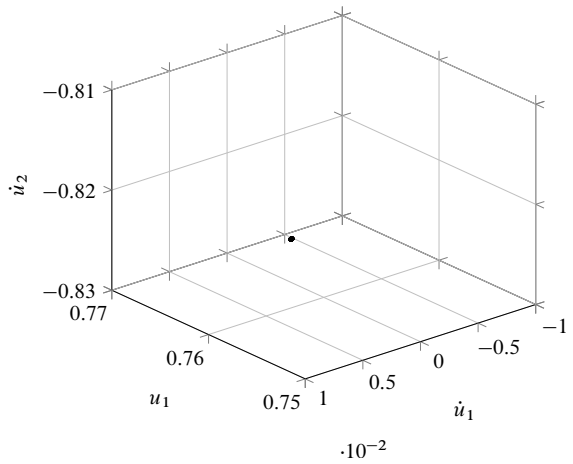

Figure 12. Post-impact Poincaré section at t^+_{imp} in the vicinity of the linear orbit at $\Omega = 1.43$. In agreement with Figure 10, the considered orbit is neutrally stable as most points on the Poincaré section are confined to a very small domain which includes the initial condition.

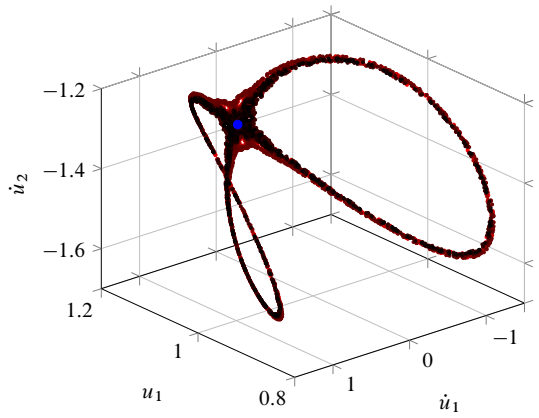

Figure 13. Post-impact Poincaré section at t^+_{imp} in the vicinity of the linear orbit at $\Omega = 1.51$. Initial condition indicated as a blue dot. In agreement with Figure 10, the considered orbit is unstable and surrounded by a chaotic-like response most probably.

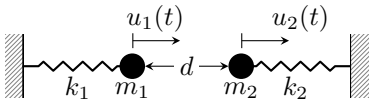

Figure 14. Two 1-degree-of-freedom oscillators interacting through unilateral contact.

$$\mathbf{M} = \begin{bmatrix} m_1 & 0 \\ 0 & m_2 \end{bmatrix} \quad \text{and} \quad \mathbf{K} = \begin{bmatrix} k_1 & 0 \\ 0 & k_2 \end{bmatrix} \tag{38}$$

and the linear modes read $\mathbf{u}_1 = [1\ 0]^\top$ and $\mathbf{u}_2 = [0\ 1]^\top$. Then, through the change of variables

$$\begin{pmatrix} v_1 \\ v_2 \end{pmatrix} = \begin{bmatrix} 1 & 1 \\ 1 & -1 \end{bmatrix} \begin{pmatrix} u_1 \\ u_2 \end{pmatrix} \tag{39}$$

the governing equations exposed in the preceding sections are recovered with the new matrices

$$\mathbf{M}_{\text{new}} = \frac{1}{2} \begin{bmatrix} m_1 + m_2 & m_1 - m_2 \\ m_1 - m_2 & m_1 + m_2 \end{bmatrix} \quad \text{and} \quad \mathbf{K}_{\text{new}} = \frac{1}{2} \begin{bmatrix} k_1 + k_2 & k_1 - k_2 \\ k_1 - k_2 & k_1 + k_2 \end{bmatrix} \tag{40}$$

and the unilateral contact condition acts on $v_2 = u_1 - u_2 \leq d$.

By properly choosing the stiffnesses k_1, k_2 and masses m_1, m_2, it is possible to achieve $\omega_2 = \omega_1$

(with $k_1 = k_2$ and $m_1 = m_2$) with the following consequences:

$$\mathbf{\Phi}(T) = \begin{bmatrix} \dfrac{\sin\omega_1 T}{\omega_1(1-\cos\omega_1 T)} & 0 \\ 0 & \dfrac{\sin\omega_1 T}{\omega_1(1-\cos\omega_1 T)} \end{bmatrix} \tag{41}$$

and

$$\mathbf{w}(T) = \begin{pmatrix} 0 \\ \dfrac{\sin\omega_1 T}{\omega_1(1-\cos\omega_1 T)} \end{pmatrix} \tag{42}$$

that is

$$\begin{pmatrix} v_1(0) \\ v_2(0) \\ \dot{v}_1(0) \\ \dot{v}_2^+(0) \end{pmatrix} = d \begin{pmatrix} 0 \\ 1 \\ 0 \\ \dfrac{\omega_1(1-\cos\omega_1 T)}{\sin\omega_1 T} \end{pmatrix} \tag{43}$$

and the results exposed in Section 2 for the one-degree-of-freedom oscillator are recovered. The nonlinear system features a single backbone curve and the classical superabundance of modes is thus destroyed by the internal resonance condition even though the two linear modes really interact together since $v_1 = u_1 + u_2 = 0$, that is $u_1 = -u_2$, as expected due to the symmetry in the chosen system.

The condition $\omega_2 = 2\omega_1$ can be achieved with $k_2 = 4k_1$ and $m_1 = m_2$ with the consequences that

$$\mathbf{\Phi}(T) = \begin{bmatrix} \dfrac{\sin\omega_1 T}{\omega_1(1-\cos\omega_1 T)} & 0 \\ 0 & \dfrac{\sin 2\omega_1 T}{2\omega_1(1-\cos 2\omega_1 T)} \end{bmatrix} \tag{44}$$

and

$$\mathbf{w}(T) = \begin{pmatrix} -\dfrac{\cos\omega_1 T + 2}{4\omega_1 \sin\omega_1 T} \\ \dfrac{3\cos\omega_1 T + 2}{4\omega_1 \sin\omega_1 T} \end{pmatrix} \tag{45}$$

that is

$$\begin{pmatrix} v_1(0) \\ v_2(0) \\ \dot{v}_1(0) \\ \dot{v}_2^+(0) \end{pmatrix} = d \begin{pmatrix} -\dfrac{\cos\omega_1 T + 2}{3\cos\omega_1 T + 2} \\ 1 \\ 0 \\ \dfrac{4\omega_1 \sin\omega_1 T}{3\cos\omega_1 T + 2} \end{pmatrix}. \tag{46}$$

Since $\omega_2 = 2\omega_1$, the sub-harmonic 2 of the second mode (green curve in Figure 8) disappears and overlaps with the backbone curve of the first mode (red curve in Figure 8) and it can be shown numerically that only the two backbone curves corresponding to modes 1 and 2 exist. Also, at $\omega_1 T = 2\pi$, we have $\omega_2 T = 2\omega_1 T = 4\pi$ and it is possible to show that the kernel of the operator (23) has dimension higher than 1, in contrast to the preceding configurations. The consequence is that the connection of the nonlinear backbone curve with its linear counterpart (the purely vertical portion located at ω_1) is no longer clearly defined and the investigation should be dealt with in more details. Also, such internal resonances do not manifest themselves in the above manner for smooth nonlinear systems.

4 Conclusion and Perspectives

To conclude this short chapter, we would like to state again the existence of a zoology of interesting phenomena in nonlinear dynamics, and more specifically in the field of nonlinear modal analysis, that have commonly no counterparts in the linear framework, among which: frequency-energy dependence in modal motions, curved invariant manifolds of periodic orbits in the state-space, superabundance of modes, bifurcation mechanisms, and internal resonances. Each of these topics was briefly discussed through simple vibro-impact autonomous oscillators which enjoy quasi-exact solutions. The chapter did not cover periodic solutions with multiple impacts per period (Thorin et al., 2017), which a topic in itself. Finally, the classical questions about the relationships between backbone curves and periodically forced responses were not addressed. Many aspects are still open, notably concerning grazing solutions around which intricate bifurcation mechanisms arise and internal resonances.

Acknowledgments The author would like to dedicate this chapter to his collaborators S. Junca and A. Thorin for their joint work and uncountable discussions, without which the material of this chapter would not exist.

Supplementary material The Matlab scripts used to generate the results shown in this chapter are available at the permalink `https://hal.science/hal-04599802`.

Bibliography

Vincent Acary and Bernard Brogliato. *Numerical Methods for Nonsmooth Dynamical Systems: Applications in Mechanics and Electronics*, volume 35 of *Lecture Notes in Applied and Computational Mechanics*. Springer, 2008. doi:10.1007/978-3-540-75392-6. URL `https://inria.hal.science/inria-00423530`.

Heiko Gimperlein, Fabian Meyer, Özdemir Ceyhun, and Ernst Stephan. Time domain boundary elements for dynamic contact problems. *Computer Methods in Applied Mechanics and Engineering*, 333:147–175, 2018. doi:10.1016/j.cma.2018.01.025. URL `https://hal.science/hal-01509452`.

Sami Karkar, Bruno Cochelin, and Christophe Vergez. A comparative study of the harmonic balance method and the orthogonal collocation method on stiff nonlinear systems. *Journal of Sound and Vibration*, 333 (12):2554–2567, 2014. doi:10.1016/j.jsv.2014.01.019. URL `https://hal.science/hal-01065672`.

Dominik Kern. A simple time-stepping scheme for the bouncing ball example. 2019. Unpublished, doi:10.5281/zenodo.13968927.

Houari Boumediène Khenous, Patrick Laborde, and Yves Renard. Mass redistribution method for finite element contact problems in elastodynamics. *European Journal of Mechanics - A/Solids*, 27(5):918–932, 2008. doi:10.1016/j.euromechsol.2008.01.001. URL `https://hal.science/hal-00582045`.

Mathias Legrand, Stéphane Junca, and Sokly Heng. Nonsmooth modal analysis of a N-degree-of-freedom system undergoing a purely elastic impact law. *Communications in Nonlinear Science and Numerical Simulation*, 45:190–219, 2017. doi:10.1016/j.cnsns.2016.08.022. URL `https://hal.science/hal-01185980`.

Ludovic Renson, Gaëtan Kerschen, and Bruno Cochelin. Numerical computation of nonlinear normal modes in mechanical engineering. *Journal of Sound and Vibration*, 2016. doi:10.1016/j.jsv.2015.09.033. URL `https://hal.science/hal-01380577`.

Olivier Thomas. Understanding, computing and identifying the nonlinear dynamics of elastic and piezoelectric structures thanks to nonlinear modes. In *Model Order Reduction for Design, Analysis and Control of Nonlinear Vibratory Systems*. Springer, 2024. doi:10.1007/978-3-031-67499-0_4. URL `https://hal.science/hal-04596527`.

Anders Thorin, Pierre Delezoide, and Mathias Legrand. Non-smooth modal analysis of piecewise-linear impact oscillators. *SIAM Journal on Applied Dynamical Systems*, 16(3):1710–1747, 2017. doi:10.1137/16M1081506. URL `https://hal.science/hal-01298983`.

Cyril Touzé, Alessandra Vizzaccaro, and Olivier Thomas. Model order reduction methods for geometrically nonlinear structures: a review of nonlinear techniques. *Nonlinear Dynamics*, 105, 2021. doi:10.1007/s11071-021-06693-9. URL `https://hal.science/hal-03283647`.

Cyril Touzé and Alessandra Vizzaccaro. Nonlinear normal modes as invariant manifolds for model order reduction. In *Model Order Reduction for Design, Analysis and Control of Nonlinear Vibratory Systems*. Springer, 2024. doi:10.1007/978-3-031-67499-0_2. URL `https://hal.science/hal-04594345`.